Neuro-Oncology

Neuro-Oncology 17(12), 1637–1647, 2015
doi:10.1093/neuonc/nov099
Advance Access date 23 September 2015

Diagnostic and prognostic value of ^{18}F-DOPA PET and ^{1}H-MR spectroscopy in pediatric supratentorial infiltrative gliomas: a comparative study

Giovanni Morana, Arnoldo Piccardo, Matteo Puntoni, Paolo Nozza, Armando Cama, Alessandro Raso, Samantha Mascelli, Michela Massollo, Claudia Milanaccio, Maria Luisa Garrè, and Andrea Rossi

Istituto Giannina Gaslini, Genova, Italy (G.M., P.N., A.C., A.R., S.M., C.M., M.L.G., A.R.); Nuclear Medicine Unit, Ospedali Galliera, Genova, Italy (A.P., M.M.); Clinical Trial Unit, Scientific Directorate, Ospedali Galliera, Genova, Italy (M.P.)

Corresponding Author: Giovanni Morana, MD, Neuroradiology Unit, Istituto Giannina Gaslini, Largo G. Gaslini 5, 16147 Genova, Italy (giovannimorana@ospedale-gaslini.ge.it).

Background. ^{1}H-MR spectroscopy (MRS) and ^{18}F-dihydroxyphenylalanine (DOPA) PET are noninvasive imaging techniques able to assess metabolic features of brain tumors. The aim of this study was to compare diagnostic and prognostic information gathered by ^{18}F-DOPA PET and ^{1}H-MRS in children with supratentorial infiltrative gliomas or nonneoplastic brain lesions suspected to be gliomas.

Methods. We retrospectively analyzed 27 pediatric patients with supratentorial infiltrative brain lesions on conventional MRI (21 gliomas and 6 nonneoplastic lesions) who underwent ^{18}F-DOPA PET and ^{1}H-MRS within 2 weeks of each other. ^{1}H-MRS data (choline/N-acetylaspartate, choline-to-creatine ratios, and presence of lactate) and ^{18}F-DOPA uptake parameters (lesion-to-normal tissue and lesion-to-striatum ratios) were compared and correlated with histology, WHO tumor grade, and patient outcome.

Results. ^{1}H-MRS and ^{18}F-DOPA PET data were positively correlated. Sensitivity, specificity, and accuracy in distinguishing gliomas from nonneoplastic lesions were 95%, 83%, and 93% for ^{1}H-MRS and 76%, 83%, and 78% for ^{18}F-DOPA PET, respectively. No statistically significant differences were found between the 2 techniques ($P > .05$). Significant differences regarding ^{18}F-DOPA uptake and ^{1}H-MRS ratios were found between low-grade and high-grade gliomas ($P \leq .001$ and $P \leq .04$, respectively). On multivariate analysis, ^{18}F-DOPA uptake independently correlated with progression-free survival ($P \leq .05$) and overall survival ($P = .04$), whereas ^{1}H-MRS did not show significant association with outcome.

Conclusions. ^{1}H-MRS and ^{18}F-DOPA PET provide useful complementary information for evaluating the metabolism of pediatric brain lesions. ^{1}H-MRS represents the method of first choice for differentiating brain gliomas from nonneoplastic lesions.^{18}F-DOPA uptake better discriminates low-grade from high-grade gliomas and is an independent predictor of outcome.

Keywords: brain tumor, DOPA, magnetic resonance spectroscopy, pediatric, PET.

Conventional MRI represents the backbone of brain tumor identification and characterization but has limitations in distinguishing tumors from tumor mimics, defining tumor grade, and predicting patient outcome. Complementary imaging biomarkers capable of providing a more reliable, and possibly quantitative, evaluation of biological activity are needed to further improve the clinical management of affected patients. ^{1}H-MR spectroscopy (MRS) and positron emission tomography (PET) are noninvasive imaging techniques providing insight into the metabolic behavior of brain lesions. ^{1}H-MRS estimates the levels of various metabolites within brain tissue that may be helpful for differentiating neoplastic from nonneoplastic lesions and evaluating tumor aggressiveness.[1–3]

PET imaging provides further complementary insights into tumor biology and vitality. Depending on the radiotracer used, various molecular processes can be visualized, and a growing body of evidence supports the promising role of radiopharmaceuticals that target amino acid transport.[4–6] PET imaging of brain tumors with amino acid analogs has proven advantageous over ^{18}F-fluorodeoxyglucose (FDG) because of the higher uptake in tumor tissue and lower uptake in normal brain tissue. Furthermore, as brain tumor uptake of amino acid

Received 14 February 2015; accepted 5 May 2015

tracers is predominantly determined by expression and activity of the L-amino acid transporter system, brain tumor visualization and characterization does not depend on the status of the blood-brain barrier, thus allowing amino acid uptake to occur in both enhancing and nonenhancing tumor components.[6,7]

At present, ^{11}C-methionine (MET) and ^{18}F-FDG are the best-studied tracers in children.[8,9] However, in the last few years, ^{18}F-dihydroxyphenylalanine (DOPA) has been proposed as an alternative radiolabeled tracer for characterizing pediatric brain tumors.[10,11]

Although several studies have evaluated the role of ^{1}H-MRS or PET into various aspects of brain tumor imaging including tumor diagnosis, treatment planning, and posttreatment surveillance, a limited number of investigations have compared the amount of information obtained by these different imaging modalities in both adults and children.[12–17] In particular, no prior studies have examined ^{18}F-DOPA PET and ^{1}H-MRS data in the same population of patients.

On the basis of these considerations, the overall objective of this retrospective study was to analyze metabolic information obtained by ^{18}F-DOPA PET and ^{1}H-MRS in a population of children with supratentorial infiltrative gliomas or nonneoplastic brain lesions that were initially suspected to be gliomas on conventional MRI. Specifically, we aimed (i) to compare sensitivity, specificity, and accuracy of ^{1}H-MRS and ^{18}F-DOPA PET in distinguishing brain gliomas from nonneoplastic lesions, (ii) to assess the ability of ^{1}H-MRS and ^{18}F-DOPA PET for discriminating low-grade from high-grade gliomas, and (iii) to evaluate the relationship between these different metabolic biomarkers and patient outcome in terms of progression-free survival (PFS) and overall survival (OS).

Materials and Methods

Participants

A retrospective review was conducted on all pediatric patients referred to our institution between 2009 and 2014 for histologically proven supratentorial gliomas or nonneoplastic brain lesions, which were initially suspected to be gliomas on conventional MRI, and who underwent MRI (including ^{1}H-MRS) and ^{18}F-DOPA PET within 2 weeks of each other. Specifically, we included patients younger than aged 18 years in whom the PET study had been performed due to the presence of an infiltrating lesion on conventional MRI.

Some of these patients had been enrolled in a prospective pilot study aimed at evaluating the clinical role of ^{18}F-DOPA PET/MR image fusion in children with infiltrative astrocytomas.[10]

Twenty-seven (15 males and 12 females) participants were identified. Patient age ranged from 4 to 17 years (average: 10 y). The main characteristics of the participants and their brain lesions (21 infiltrative gliomas and 6 nonneoplastic lesions) are summarized in Table 1. Among participants with gliomas, 20 of 21 were newly diagnosed and had undergone no previous treatment except for biopsy; the remaining patient was a child with a known stable residual ganglioglioma. This child had been previously treated with surgery, chemotherapy, and radiotherapy and suddenly developed an infiltrating mass lesion that turned out to be an anaplastic ganglioglioma.

The diagnosis was histologically confirmed in all but 2 participants with nonneoplastic lesions, whose final diagnosis of postsurgical/posttherapeutic changes was based on imaging follow-up (24 months) and clinical criteria. These 2 children (cases 22 and 24, Table 1) had been operated for glioma and subsequently developed a lesion adjacent to the operative site that was considered suspicious for tumor recurrence by conventional MRI (Supplementary material, Figure S1).

Neoplastic lesions underwent molecular analyses to evaluate both of the 2 common mutations (K27M and G34R/V) in the histone variant H3.3 (H3F3A) and the R132H mutation of the NADP+-dependent isocitrate dehydrogenase-1 (IDH1) (see Supplementary Materials and Methods for details). Mutations in H3F3A were evaluated in high-grade lesions. In this analysis, we also included the participant with gliomatosis cerebri, WHO grade II, who underwent disease progression (case 4). Among the 11 high-grade gliomas included in our study, the biological material from 2 participants was not available. In all, 9 of 11 high-grade gliomas were tested. IDH1 mutation was tested in 18 of the 21 participants (biological material of one low-grade and 2 high-grade lesions was not available) (Table 1).

Written informed consent was signed by all participants or their legal guardians, and patient assent was obtained whenever appropriate. The Institutional Review Board approved the study.

Image Protocol and Analysis

^{18}F-DOPA PET was carried out 20 minutes after injection of 185 MBq of ^{18}F-DOPA in all participants. ^{18}F-DOPA was purchased from a commercial supplier (IASOdopa, IASON Labormedizine Ges.Mbh & Co. KG). Data were acquired in 3-dimensional mode on a dedicated PET/CT system (Discovery ST, GE Medical Systems) with a scanning time of 30 minutes. The participants fasted for at least 4 hours before ^{18}F-DOPA PET. Carbidopa premedication was not utilized. A nondiagnostic, low-dose CT scan (120 kV, 80 mA, 0.6 s per rotation) was used for attenuation correction.

MRI studies were performed on a 1.5 Tesla magnet (Intera Achieva, Philips). The routine brain MRI examination consisted of axial fluid attenuation inversion recovery (FLAIR), T2- and T1-weighted images, and coronal T2-weighted images. Following gadolinium chelate bolus administration (0.1 mmol/kg), axial, coronal, and sagittal T1-weighted images were acquired. ^{1}H-MRS was performed simultaneously with the conventional MRI study using a single-voxel point resolved spectroscopy (PRESS) technique with an intermediate echo time of 144 milliseconds, repetition time of 2000 milliseconds, and 128 signal averages. With these parameters, the total acquisition time, including scanner adjustments, was less than 5 minutes. A cubic voxel of 1.8 cm side length was manually placed on the bulk of the lesion, according to standard diagnostic criteria, to enclose only tumor tissue and avoid or limit the inclusion of necrotic areas as much as possible. For anatomic reference, precontrast FLAIR and T2-weighted images were coregistered to ^{1}H-MRS. Spectra were generated by the internal scanner software, providing automatic peak assignation and ratio calculation. Choline-to-creatine (Cho/Cr) and choline-to-N-acetylaspartate (Cho/NAA) peak area

Table 1. Summary of patient characteristics, imaging findings and outcome

Case	Age	Sex	Diagnosis	WHO Grade	Location	H3F3A Status	IDH1 Status	CE (Y/N)	Cho/ NAA	Cho/ Cr	Lact (+/-)	L/N Spect	L/S Spect	L/N Hot	L/S Hot	Treatments Prior MRS/PET	Treatments after MRS/PET	Outcome	FU (months)
1	10	F	GNT[a]	I	L-T	ND	WT	Y	2.45	2.14	+	1.89	0.94	1.89	0.94	None	PS/CB+VC	PR	32
2	15	M	DA	II	L-Fr,T	NA	NA	N	1.60	1.70	−	1.12	0.82	1.12	0.82	None	B	PD	55
3	13	M	GC (DA)	II	R-T,Fr,P	ND	WT	N	1.90	2.50	+	1.20	0.78	1.34	0.84	B	TEM	SD	48
4	8	M	GC (DA)	II	L-T,Fr,P,BG	WT	WT	N	6.60	1.70	+	1.28	0.86	2.31	1.22	B	TEM/RT	PD	42
5	9	M	DA	II	R-P,O	ND	WT	N	4.00	1.50	+	1.00	0.60	1.00	0.60	None	B	SD	62
6	5	M	DA	II	R-T	ND	WT	N	3.10	1.10	+	0.98	0.55	0.98	0.55	None	B	SD	12
7	11	F	DA	II	R-T,Fr	ND	WT	N	2.50	1.80	−	1.51	0.83	1.51	0.83	B	RT	PR	25
8	14	M	DA	II	R-P,CC	ND	WT	N	1.30	1.10	−	1.00	0.40	1.00	0.40	None	B	SD	26
9	10	M	DA	II	R-Fr	ND	WT	N	1.20	1.00	−	0.91	0.51	0.91	0.51	None	B	SD	46
10	12	F	DA	II	L-Fr	ND	WT	N	1.00	0.90	−	1.00	0.51	1.00	0.51	None	PS/CB+VC	PR	63
11	16	F	AA	III	L-R-Th	NA	NA	N	3.90	1.50	−	3.41	1.40	3.41	1.40	B	TEM/RT	PD and DOD	9
12	14	M	AA	III	L-T,P	K27M	WT	N	2.20	1.80	+	2.04	1.14	2.04	1.14	None	SS/TEM/RT	PD and DOD	19
13	7	F	AA	III	L-Fr,P	WT	WT	N	3.50	2.00	+	1.41	0.87	2.31	1.25	B	SS/TEM/RT	PD and DOD	6
14	8	F	AGG[b]	III	L-T	WT	WT	N	4.58	8.99	+	2.10	1.40	2.10	1.40	PS/CB+VC/RT	PS/TEM+BEV	PD and DOD	8
15	10	M	GC (AA)	III	L-Fr,P,BG, R-Fr,P	WT	WT	N	1.39	1.13	+	1.72	1.23	1.72	1.23	None	B/TEM/RT	PD	13
16	6	F	AA	III	R-T,Fr	WT	WT	N	3.20	2.20	+	1.44	0.79	1.73	1.22	None	PS/TEM/RT	PD and DOD	10
17	17	F	GBM	IV	L-T,Fr	NA	NA	N	7.30	2.70	−	2.34	1.22	2.34	1.22	B	TEM/RT	PD and DOD	33
18	8	M	GBM	IV	R-T,O,BG	WT	WT	Y	3.07	7.26	−	2.13	1.39	2.13	1.39	None	PS/TEM/RT	PD and DOD	4
19	5	M	GBM	IV	L-Th	WT	WT	Y	5.30	4.20	+	1.83	0.96	2.26	1.21	None	PS/TEM/RT	PD and DOD	10
20	8	M	GBM	IV	L-Fr,P,BG	WT	WT	Y	5.40	1.45	+	2.22	1.31	2.32	1.43	B	TEM/RT	PD and DOD	9
21	6	F	GBM	IV	R-DMJ,BG	WT	WT	Y	3.90	9.80	−	2.23	1.58	2.23	1.58	None	PS/TEM/RT	PD and DOD	8
22	17	M	Post therapeutic changes (suspected AA recurrence)	/	R-Fr	/	/	N	0.95	1.93	+	0.89	0.52	0.89	0.52	TS/TEM/RT	None	/	/
23	5	M	Gliosis	/	R-Fr	/	/	N	0.62	1.34	−	0.82	0.43	0.82	0.43	None	B	/	/
24	11	M	Post therapeutic changes (suspected DA recurrence)	/	L-Fr	/	/	N	0.85	1.31	−	0.87	0.47	0.87	0.47	TS	None	/	/
25	15	F	Gliosis	/	R-P	/	/	N	0.78	1.92	−	0.97	0.34	0.97	0.34	None	B	/	/
26	4	F	Encephalitis	/	L-Fr,BG	/	/	N	1.22	1.66	−	1.88	1.25	1.88	1.25	None	B	/	/
27	10	F	Meningioangiomatosis	/	R-Fr	/	/	N	0.64	1.35	−	0.93	0.48	0.93	0.48	None	SS	/	/

Abbreviations: AA, anaplastic astrocytoma; AGG, anaplastic ganglioglioma; B, biopsy; BEV, bevacizumab; BG, basal ganglia; CB, carboplatin; CC, corpus callosum; CE, contrast enhancement; DA, diffuse astrocytoma; DMJ, diencephalic-mesencephalic junction; DOD, died of disease; F, female; Fr, frontal; FU, follow-up; GBM, glioblastoma multiforme; GC, gliomatosis cerebri; GNT, glioneuronal tumor; L, left; M, male; NA, not available; ND, not done; O, occipital; P, parietal; PD, progressive disease; PR, partial response; PS, partial surgery; R, right; RT, radiotherapy; SD, stable disease; SS, subtotal surgery; T, temporal; TEM, temozolomide; Th, thalamus; TS, total surgery; VC, vincristine; WT, wild type.
[a]Lesion with a prominent infiltrating glial population composed of astrocytic cells resembling a fibrillary astrocytoma and neoplastic ganglion cells.
[b]Anaplastic infiltrating lesion developing from a small residual ganglioglioma treated 2 years before.

ratios were recorded. For each ^{1}H-MRS study, the presence of lactate, defined by prominent peak (signal: noise >3:1) between 1.3 and 1.4 ppm, was also assessed. ^{1}H-MRS was considered positive if the Cho/NAA ratio was greater than 1. Although there is no standardized classification of tumors based on ^{1}H-MRS, this threshold value was selected on the basis of prior studies of ^{1}H-MRS biomarkers in pediatric patients with brain tumors.[14,18]

All ^{18}F-DOPA-PET studies were interpreted qualitatively and semiquantitatively, coregistering and fusing the images with MRI. PET/MRI coregistration and fusion were obtained semiautomatically using a commercially available registration image software tool (Xeleris, GE Healthcare). ^{18}F-DOPA PET images were coregistered and fused to axial FLAIR and T2-weighted images. PET scans were classified as positive if lesions identified on MRI exhibited tracer uptake above the level of the corresponding contralateral normal brain tissue.[11]

Since single voxel ^{1}H-MRS gives metabolic information of a limited part of the lesion while PET imaging allows whole brain and lesion coverage, we compared metabolic data obtained by the ^{1}H-MRS volume of interest (VOI) with the metabolic information gathered by DOPA PET in the matching area. To do so, the precontrast T2 and FLAIR images coregistered to the ^{1}H-MRS and ^{18}F-DOPA PET data were the common anatomical references for the 2 techniques. Furthermore, we evaluated whether the VOI selected for ^{1}H-MRS in the bulk of the lesion included the area with maximum tracer uptake on PET. If not, additional PET metabolic information was obtained from the area displaying the maximum uptake. In detail, a square-shaped region of interest (ROI) of 1.8×1.8 cm was manually drawn over the lesion area corresponding to the center of ^{1}H-MRS VOI (L Spect). If this ROI did not include the area displaying the highest ^{18}F-DOPA PET uptake, an additional same-sized ROI was drawn over the lesion hot spot (L Hot). In case of negative ^{18}F-DOPA PET, the ROI corresponded to the center of the ^{1}H-MRS VOI. The radiotracer concentration in the ROIs was normalized to the injected dose per patient's body weight, and the maximum standardized uptake value (SUVmax; g/mL) was obtained for each ROI. For the normal reference tissue, a ROI of the same size was mirrored to the matching contralateral normal brain (N). Another ROI was drawn over the contralateral normal striatum (S). Ratios of lesion-to-normal-tissue uptake were generated by dividing the SUVmax obtained from the lesional ROIs (SUVmax in the area matching the MRS VOI and SUVmax from the lesion hot spot if different), by the SUVmax of the contralateral normal brain region (L/N Spect and L/N Hot) and of the normal striatum (L/S Spect and L/S Hot). Results of only one ^{1}H-MRS and ^{18}F-DOPA PET study were analyzed per participant.

The contrast enhancement pattern of the lesions was also reviewed to evaluate the relationship between ^{18}F-DOPA accumulation and the blood-brain barrier status.

Disease Monitoring and Outcome analysis

To monitor the disease status and outcome, we relied upon clinical and MRI methods according to Response Assessment in Neuro-oncology (RANO) criteria for high-grade and low-grade gliomas.[19,20] Tumor size was assessed using the diameter method, as previously described.[21]

The median follow-up time available for all participants with brain gliomas was 19 months (range: 4–63 mo). In particular, it was 44 months (range: 12–63 mo) for WHO grade I/II gliomas and 9.5 months (range: 4–33 mo) for WHO grade III/IV gliomas. All participants with grade I/II gliomas were alive, whereas all but one with grade III/IV gliomas had died by the time this study was completed.

Statistical Analysis

Descriptive statistics included mean, standard deviation, median, percentiles, minimum, and maximum of continuous factors and scores; in the case of categorical factors, number and percentage distribution were used. Pearson's chi-square and Kruskal-Wallis or Mann-Whitney *U* tests were used to compare categorical and continuous factors, respectively. Spearman's rank correlation coefficient was used to test the correlation between parameters; sensitivity, specificity, positive predictive value, negative predictive value, and diagnostic accuracy were used for descriptive purposes. Sensitivity was defined as the proportion of true positive (TP) tests to the total number of positive (as defined in the Image Protocol and Analysis section) participants tested. Specificity was defined as the ratio of true negative (TN) tests to the total number of negative participants. We defined diagnostic accuracy (effectiveness) as the proportion of correctly classified participants (TP + TN) among all participants. Kaplan-Meier estimates of the cumulative probability of PFS and OS (defined as the interval between initial diagnosis and the onset of disease progression and of death from any cause, respectively) were obtained. Each parameter was categorized considering tertiles of each distribution, and log-rank test for trend was applied. The Cox proportional hazard model was used to estimate the risk of disease progression and death from any cause after adjustment for age, sex, tumor grade, and tumor dimension. The proportional hazard assumption was graphically checked. Since the parameters were highly correlated, to avoid collinearity, we used different models for each parameter to test their independent association with PFS and OS. Since each parameter was tested as a continuous variable in the model, hazard ratios refer to the increase of one point of each parameter.

All analyses were conducted using Stata (version 13, StataCorp) software. Two-tailed probabilities were reported, and a *P* value of .05 was used to define nominal statistical significance.

Results

Diagnostic Evaluation

^{18}F-DOPA PET was positive in 17 of 27 lesions (one false positive). Among the 10 negatives PET scans were 5 true negatives and 5 false negatives. Sensitivity, specificity, and accuracy were 76%, 83%, and 78%, respectively. All false negative ^{18}F-DOPA PET lesions were low-grade diffuse astrocytomas. The false positive lesion turned out to be encephalitis.

^{1}H-MRS was positive in 21 of 27 lesions (one false positive). Among the 6 negative ^{1}H-MRS lesions were 5 true negatives and one false negative. Sensitivity, specificity, and accuracy were 95%, 83%, and 93%, respectively. The false negative ^{1}H-MRS lesion was a low-grade diffuse astrocytoma, whereas

the false positive was the same encephalitis case also detected by ^{18}F-DOPA PET. Positive predictive value and negative predictive value were 94% and 50% for ^{18}F-DOPA PET, and 95% and 83% for ^{1}H-MRS. No statistically significant differences were demonstrated between the 2 techniques ($P > .05$).

Positive correlation was found between ^{18}F-DOPA PET uptake in the area corresponding to the ^{1}H-MRS VOI (L/N Spect and L/S Spect ratios) and ^{1}H-MRS metabolite parameters (Cho/NAA and Cho/Cr ratios) (Fig. 1). In 6 of 21 tumoral lesions, the VOI selected for ^{1}H-MRS did not include the area with the highest ^{18}F-DOPA uptake; these participants presented with extensive, heterogeneous lesions (2 glioblastomas, 2 anaplastic astrocytomas, and 2 gliomatosis cerebri). ^{18}F-DOPA PET uptake (L/N Hot, L/S Hot, L/N Spect, L/S Spect) and ^{1}H-MRS (Cho/Cr, Cho/NAA, presence of lactate) data of all lesions are reported in Table 1. ^{18}F-DOPA accumulated in enhancing and nonenhancing lesions, and there was no apparent association between the degree of DOPA uptake and the contrast-enhancement (Table 1).

A strong statistically significant difference regarding ^{18}F-DOPA uptake was found between low-grade and high-grade tumors ($P \leq .001$) (Fig. 2A–D). A statistically significant difference regarding Cho/NAA and Cho/Cr ratios was also found between low-grade and high-grade gliomas ($P \leq .04$), although differences in medians of ^{1}H-MRS ratios were lower than those for ^{18}F-DOPA uptake (Fig. 2E and F). A lactate peak on ^{1}H-MRS was found in 5 of 10 low-grade tumors (50%) and in 7 of 11 high-grade tumors (63%). No statistically significant difference was demonstrated between DOPA uptake and presence of lactate (L/S Spect and lactate, $P = .23$; L/N Spect and lactate, $P = .49$).

Molecular analysis revealed no IDH1 mutations. None of the analyzed tumor entities showed G34R/V mutation, while one of 9 cases (11%) harbored K27M mutation (case 12, Table 1). Representative images of nonneoplastic and neoplastic lesions are shown in Fig. 3.

Prognostic Evaluation

After a median clinical and imaging follow-up time of 19 months (range: 4–63 mo), a total of 13 disease progressions and 10 deaths were observed. Figure 4 shows Kaplan-Meier OS curves for all of the main factors analyzed in our study. Participants with higher L/S and L/N had a significantly higher risk of disease progression (data not shown, $P < .005$) and death (Fig. 4A–D, $P \leq .004$) than those with lower L/S and L/N values. This finding was observed not only when considering the lesion hot spot (L/S Hot and L/N Hot) but also when analyzing ^{18}F-DOPA uptake in the area matching the MRS VOI (L/S Spect and L/N Spect). At the same time, we found that, at univariate level, participants with higher tumor grade (WHO grade I-II vs III-IV) had a significantly higher risk of disease progression (data not shown, $P < .001$) and death (Fig. 4E, $P < .001$). Participants with larger lesions (maximum diameter <60 mm vs >60 mm) had a significantly higher risk of disease progression (data not shown, $P = .001$) but no higher risk of death (Fig. 4F, $P = .2$). Regarding ^{1}H-MRS parameters, participants

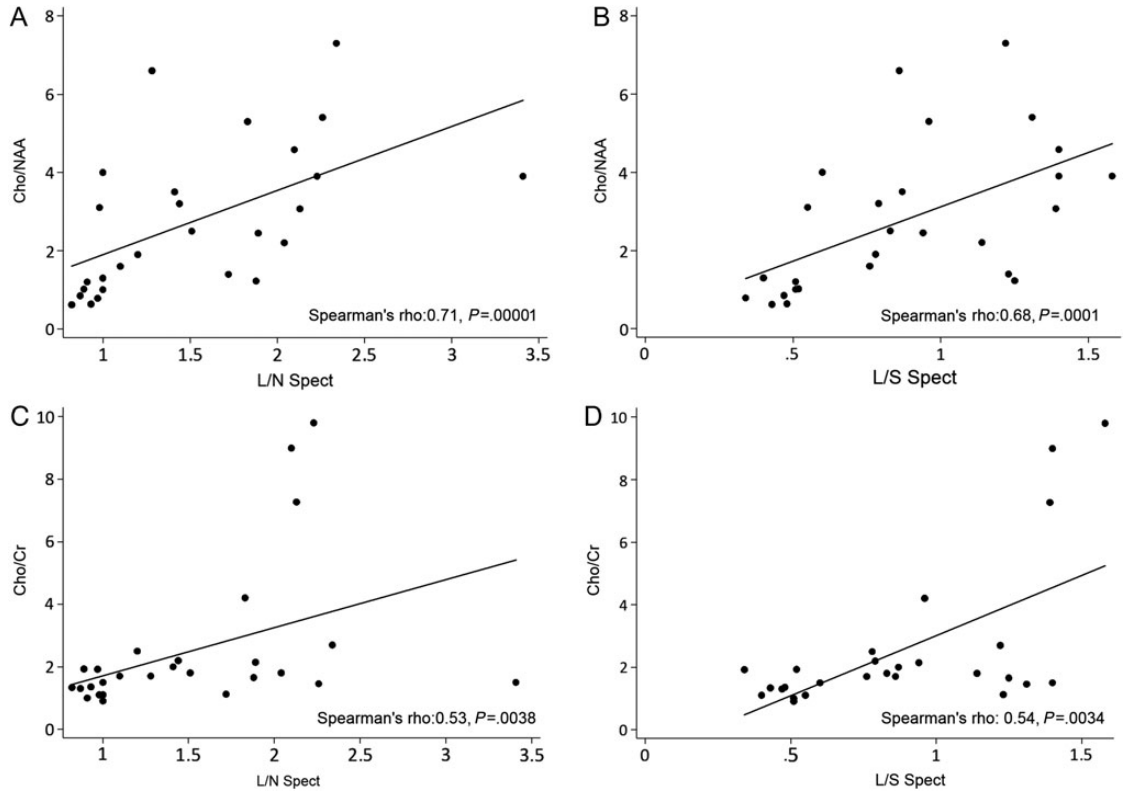

Fig. 1. Linear regression analysis of ^{18}F-DOPA uptake and ^{1}H-MRS ratios. All parameters are positively correlated. The strongest correlation is demonstrated between Cho/NAA and L/N Spect ratios (A).

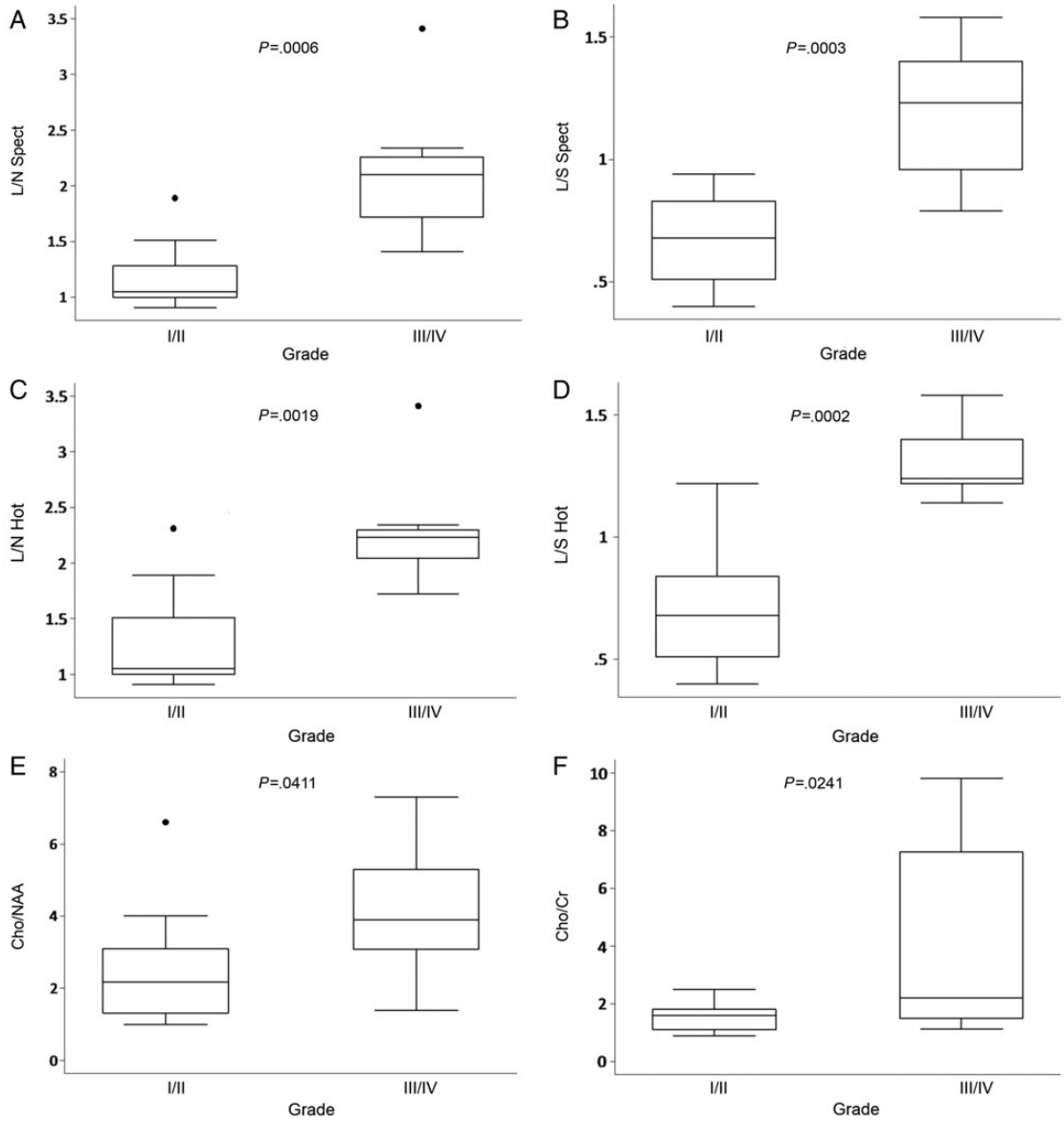

Fig. 2. Box plots representing ^{18}F-DOPA uptake (A–D) and ^{1}H-MRS ratios (E, F) for low-grade and high-grade gliomas.

with higher Cho/NAA ratios did not show significantly higher risk of disease progression (data not shown, $P = .2$) and death (Fig. 4G, $P = .09$) than those with lower Cho/NAA ratios. By contrast, the participants with higher Cho/Cr ratios showed higher risk of death (Fig. 4H, $P = .03$) than those with lower Cho/Cr ratios. However, when we adjusted risk estimates for age, sex, tumor dimensions, and tumor grade by using a multivariate Cox model, only L/S Hot ($P = .05$), L/N Hot ($P = .02$), and L/N Spect ($P = .005$) remained independently associated with PFS (Table 2). Considering OS multivariate Cox models, despite the low power due to the limited number of observed events, only L/N Spect persisted to be significantly associated with death ($P = .04$, Table 2), whereas a borderline statistically significant association was found for L/S Hot ($P = .06$) and L/N Hot ($P = .08$) parameters (data not shown on Table 2). At the multivariate level, no statistically significant association was found between MRS parameters (Cho/NAA ratio, Cho/Cr ratio, and presence of lactate), PFS ($P = .6$, $P = .8$ and $P = .6$, respectively) and OS ($P = .2$, $P = .2$ and $P = .7$, respectively).

Discussion

The objective of the present study was to compare the metabolic information gathered by ^{18}F-DOPA PET and ^{1}H-MRS in a population of children with suspected or proven infiltrative gliomas for diagnostic and prognostic purposes. ^{1}H-MRS is a well-proven diagnostic tool that allows noninvasive detection and measurement of normal and abnormal metabolites within brain tissue, indicating loss of neuroaxonal integrity and increased myelin turnover. In pediatric neuro-oncology, it has been widely applied to discriminate between brain tumors

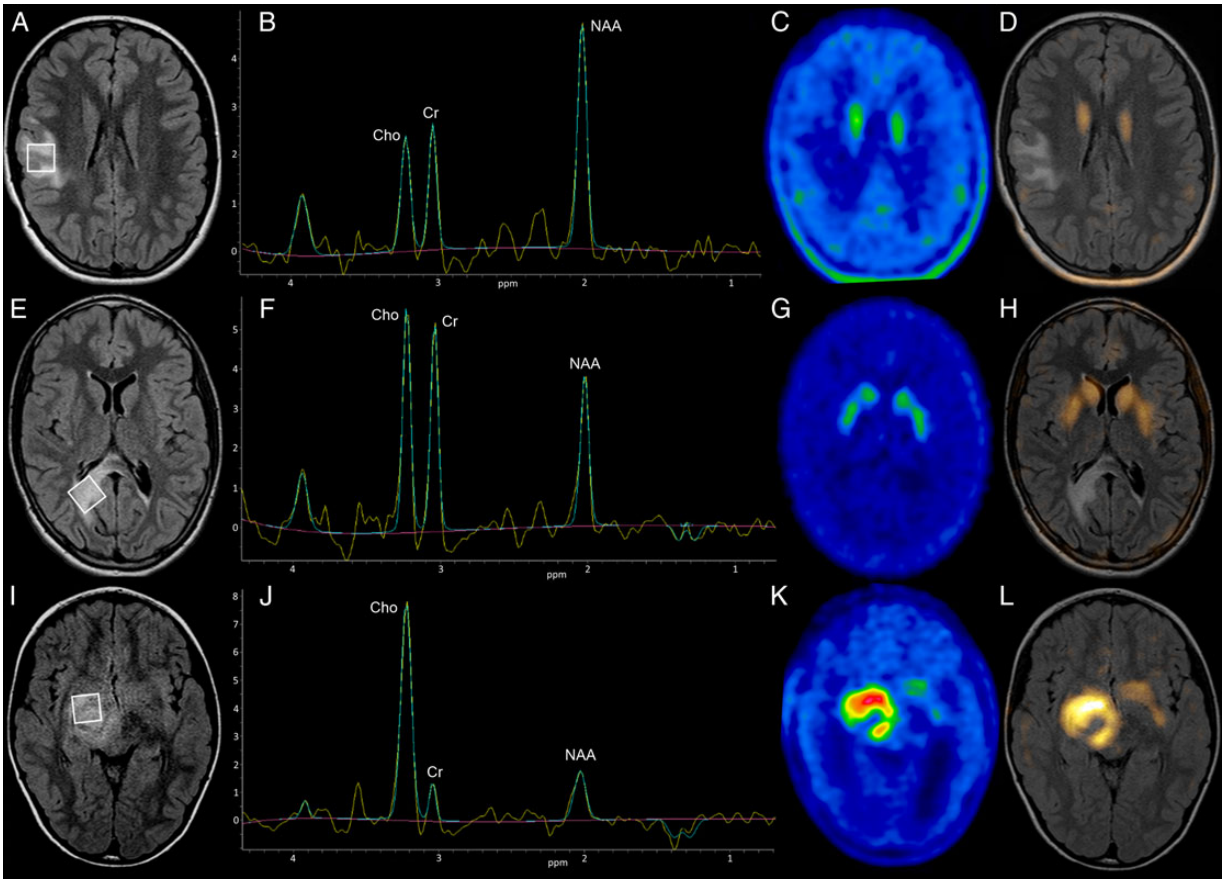

Fig. 3. MRI, ^{1}H-MRS and ^{18}F-DOPA PET images in nonneoplastic and neoplastic lesions. A–D. Meningioangiomatosis (case 27): axial FLAIR image reveals a lesion in the right frontal lobe (A). Single voxel ^{1}H-MRS (B) shows normal Cho/Cr and Cho/NAA ratios. ^{18}F-DOPA PET (C) and fused PET/MRI (D) images demonstrate absence of tracer uptake in the lesion. (E–H) Diffuse astrocytoma. WHO grade II (case 8) axial FLAIR image demonstrates a right parietal lesion extending across the splenium of the corpus callosum (E). Single voxel ^{1}H-MRS (F) shows increased Cho/NAA ratio (1,30). ^{18}F-DOPA PET (G) and fused PET/MRI (H) images show no evidence of increased uptake in the lesion. Following biopsy the patient was managed with a "watch and wait" approach, and the lesion remained stable during follow-up (26 months). I–L. Glioblastoma multiforme. WHO grade IV (case 21) axial FLAIR image reveals a lesion involving the right diencephalic-mesencephalic junction and basal ganglia (I). Single voxel ^{1}H-MRS (J) demonstrates increased Cho/NAA (3:90) and Cho/Cr (9:80) ratios. ^{18}F-DOPA PET (K), and fused PET/MRI (L) images show increased tracer uptake in the lesion (L/N: 2.23, L/S: 1.58). Following biopsy, the patient was treated with chemotherapy and radiotherapy; the OS was 8 months. Note: the box on the FLAIR images indicates the region of interest from which the spectra were acquired.

and nonneoplastic lesions, to assess tumor malignancy, and to predict survival.[22–25] Among different ^{1}H-MRS techniques, single voxel ^{1}H-MRS is quick and easy to perform and, in standard clinical settings, provides the opportunity to obtain robust data in a reasonable amount of time. Single-voxel ^{1}H-MRS has also been applied in quantitative multicenter studies.[26] Both short and long echo-time ^{1}H-MRS have been tested in pediatric brain tumors, and overall, there is no consensus on the optimal spectroscopy sequence since each has strengths and limitations. We used an echo time of 144 milliseconds because it is less sensitive to artifacts and has the advantage of providing less complex spectra that are more simple to analyze because of the flat baseline and lack of spectral overlap. Furthermore, the lactate peaks are inverted, which makes them easier to differentiate from lipids.

^{18}F-DOPA is an emerging amino-acid PET tracer for evaluating brain tumors. Cellular accumulation of ^{18}F-DOPA is mainly driven by the activity of transport systems that carry this amino acid into the tissue. L-amino acid transporter 1 expression, in particular, has been proven to be enhanced in gliomas and was found to correlate significantly with ^{18}F-DOPA uptake in human gliomas both in vitro and in vivo.[27] While several studies in adults have demonstrated the role of ^{18}F-DOPA PET in evaluating brain tumors, only a few studies have focused on pediatric brain malignancies.[10,11] To the best of our knowledge, no prior studies have compared the diagnostic and prognostic performances of ^{1}H-MRS and ^{18}F-DOPA PET in the same population of patients with brain tumors.

We found a significant positive correlation between ^{1}H-MRS data and ^{18}F-DOPA PET parameters. The strongest correlation was demonstrated between ^{18}F-DOPA uptake and the Cho/NAA ratio.This ratio has been considered the most sensitive index for tumor cell density and proliferation in prior ^{1}H-MRS studies.[28] Our diagnostic evaluation also revealed that ^{1}H-MRS was more sensitive and accurate than ^{18}F-DOPA PET in differentiating nonneoplastic lesions from brain gliomas,

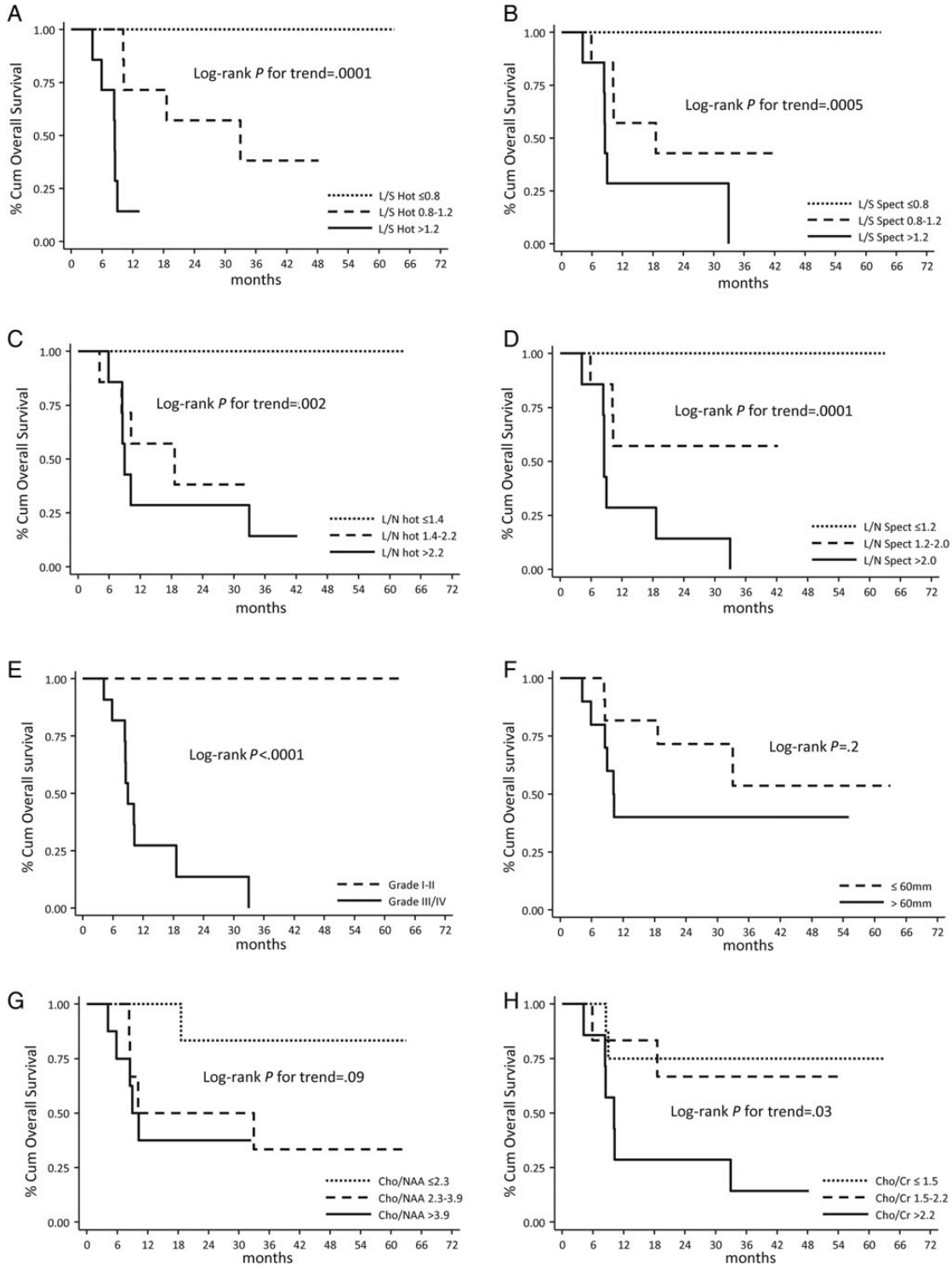

Fig. 4. Kaplan-Meier overall survival (OS) curves for all of the main factors analyzed in our study: ^{18}F-DOPA PET results. (A–D), low-grade versus high-grade gliomas (E), tumor dimension (F) and ^{1}H-MRS (G and H) results. ^{18}F-DOPA PET and ^{1}H-MRS parameters were categorized considering tertiles of each distribution.

even though these results did not reach statistical significance. These findings are in agreement with a prior study performed by Floeth et al[15] comparing single-voxel ^{1}H-MRS data with ^{18}F-fluoroethyl-L-tyrosine PET in adults with suspected brain gliomas. The lower sensitivity of ^{18}F-DOPA PET can be explained by the relatively high incidence of negative studies in pediatric

Table 2. Cox regression multivariate analyses (participants $n = 21$)

Endpoint	Parameter	HR[a]	95% CI	*P* Value
PFS (events $n = 13$)	L/N Spect	1.00		
		8.92	1.02–77.9	.005
	L/S Hot	1.00		
		237.3	1.00–56023	.05
	L/N Hot	1.00		
		9.35	1.37–63.8	.02
OS (events $n = 10$)	L/N Spect	1.00		
		16.5	1.15–238.2	.04

Abbreviations: 95%CI, 95% confidence interval; HR, hazard ratio; OS, overall survival; PFS, progression-free survival.
[a]Hazard ratios are adjusted for age, sex, tumor dimension, and tumor grade; only parameters significantly associated with the endpoint (overall survival or progression-free survival) are tabulated.

low-grade diffuse astrocytomas (5 negatives out of 7 tumors). These data differ from ^{18}F-DOPA PET results in adults with diffuse astrocytomas, in which a higher incidence of positive PET results has been reported.[7,29–31] Since pediatric low-grade diffuse astrocytomas are considered distinct and less aggressive entities when compared with their adult counterpart, the higher incidence of negative PET studies might be related to a lower expression of amino acid transporters in pediatric diffuse astrocytomas.

Both techniques revealed a false-positive result in a participant with encephalitis. Similar findings have been reported in prior ^{1}H-MRS[22] and amino acid PET[32,33] studies, suggesting a limited diagnostic value of both techniques in distinguishing brain tumors from inflammatory lesions.

The ^{18}F-DOPA uptake and ^{1}H-MRS ratios for high-grade gliomas were statistically different from those of low-grade gliomas. ^{1}H-MRS data, even when reaching a statistical significance, demonstrated a greater degree of overlap among different glioma grades. ^{18}F-DOPA uptake ratios were instead much more clustered, and all low-grade gliomas but one demonstrated a L/S ratio <1. Of note, there was no correlation between the presence of lactate and ^{18}F-DOPA uptake or tumor grade. These findings support prior evidence of a lack of correlation between evidence of lactate and pediatric brain glioma aggressiveness.[1]

Concerning prognostic information, ^{18}F-DOPA PET data differed significantly from ^{1}H-MRS. In particular, a significant relationship between ^{18}F-DOPA uptake and outcome was found both in terms of PFS and OS. ^{18}F-DOPA uptake was an independent predictor of survival on multivariate analysis. On the other hand, ^{1}H-MRS data failed to show a significant association with outcome and did not confirm prior studies in which both single- and multivoxel MRS biomarkers, particularly the Cho/NAA ratio, were found to predict patient survival.[18,23–25,34] Notably, these studies mainly included patients with different types of brain tumors, ranging from embryonal lesions to gliomas located both infratentorially and supratentorially, whereas our cohort of children with brain tumors was exclusively composed of supratentorial gliomas.

The prognostic significance of amino acid PET in pediatric gliomas has been poorly investigated. In a prior study comparing ^{18}F-FDG and ^{11}C-MET PET in pediatric brain tumors, both tracers showed prognostic significance for event-free survival in the Cox univariate regression analysis.[35] In another study including 85 children with brain tumor, ^{11}C-MET PET provided a stronger prognostic value than histology, leading to the prediction of worse evolution.[8]

Regarding molecular analyses, all tumors evaluated resulted in IDH1 wild-type in keeping with the extreme rarity of IDH1 mutation in childhood brain tumors, which was also demonstrated in a prior study by our group.[36] Only one tumor harbored the K27M mutation of H3F3A; this was a child with an hemispheric anaplastic astrocytoma whose conventional MRI, ^{1}H-MRS, and ^{18}F-DOPA PET features were not different from the other H3F3A wild-type high-grade gliomas. Of note, he presented one of the longest overall survivals (19 months) among our series of high-grade lesions; however, this result might be at least partly dependent on the location of the tumor, which allowed 90% surgical removal.

Our results should be interpreted with awareness of some limitations. A limited number of patients were studied; however, our series included only patients undergoing both ^{1}H-MRS and ^{18}F-DOPA PET, which do not represent common diagnostic procedures, especially in the pediatric population. In addition, even though we evaluated only supratentorial lesions presenting an infiltrative pattern on MRI, the study included heterogeneous lesion types. Treatment of low-grade gliomas was also heterogeneous; however, at present there is no consensus about optimal treatment strategy for low-grade diffusely infiltrating gliomas, and the participants were therefore managed based on their clinical symptoms and imaging findings. Our series was also heterogeneous concerning the timing of the PET/MRS scans, with some studies performed after biopsy; however, all participants who were biopsied prior to PET/MRS studies presented with extensive lesions where biopsies involved a minimal tumoral area without relevant influence on the postbioptic PET and MRS evaluation. We also recognize that single-voxel ^{1}H-MRS is unable to define the extent of the metabolic abnormalities in large tumors or demonstrate tissue heterogeneity. However, this technique provides robust and good-quality spectra in a relatively short period of time, compatible with standard clinical settings and patient compliance. Furthermore, since MRS VOI was placed in the bulk of the lesion, without prior knowledge of PET metabolic data, MRS sampling might not have corresponded to the higher grade areas. Nevertheless, since we analyzed ^{1}H-MRS data and ^{18}F-DOPA PET results from the same area, we were able to compare metabolic information gathered by the 2 techniques, which was the main objective of our study. Of note, even multivoxel ^{1}H-MRS might not be able to entirely cover large lesions or the entire brain within a reasonable amount of time.

In conclusion, both ^{1}H-MRS and ^{18}F-DOPA PET provide useful complementary information for evaluating the metabolism of tumor and tumor-like brain lesions in children. In view of its better availability, lower cost, and lack of radiation exposure, ^{1}H-MRS represents the method of first choice for differentiating brain gliomas from nonneoplastic lesions. ^{18}F-DOPA uptake better discriminates between low-grade and high-grade gliomas and is an independent predictor of PFS and OS.

Supplementary Material

Supplementary material is available at Neuro-Oncology Journal online (http://neuro-oncology.oxfordjournals.org/).

Funding

Funding for this work was provided by the Associazione Italiana per la Ricerca dei Tumori Cerebrali del Bambino (ARTUCEBA), the Italian Association for Cancer Research (AIRC), and Finanziamento Ricerca Corrente, Ministero Salute (contributo per la ricerca intramurale).

Conflict of interest statement. We declare that we have no conflict of interest.

References

1. Brandão LA, Castillo M. Adult brain tumors: clinical applications of magnetic resonance spectroscopy. *Neuroimaging Clin N Am*. 2013;23(3):527–555.
2. Brandão LA, Poussaint TY. Pediatric brain tumors. *Neuroimaging Clin N Am*. 2013; 23(3):499–525.
3. Rossi A, Gandolfo C, Morana G, et al. New MR sequences (diffusion, perfusion, spectroscopy) in brain tumours. *Pediatr Radiol*. 2010; 40(6):999–1009.
4. Heiss WD, Raab P, Lanfermann H. Multimodality assessment of brain tumors and tumor recurrence. *J Nucl Med*. 2011;52(10): 1585–1600.
5. La Fougère C, Suchorska B, Bartenstein P, et al. Molecular imaging of gliomas with PET: opportunities and limitations. *Neuro Oncol*. 2011;13(8):806–819.
6. Peet AC, Arvanitis TN, Leach MO, et al. Functional imaging in adult and paediatric brain tumours. *Nat Rev Clin Oncol*. 2012;9(12): 700–711.
7. Chen W, Silverman DH, Delaloye S, et al. 18F-FDOPA PET imaging of brain tumors: comparison study with 18F-FDG PET and evaluation of diagnostic accuracy. *J Nucl Med*. 2006;47(6):904–911.
8. Pirotte BJ, Lubansu A, Massager N, et al. Clinical impact of integrating positron emission tomography during surgery in 85 children with brain tumors. *J Neurosurg Pediatr*. 2010;5(5): 486–499.
9. Stanescu L, Ishak GE, Khanna PC, et al. FDG PET of the brain in pediatric patients: imaging spectrum with MR imaging correlation. *Radiographics*. 2013;33(5):1279–1303.
10. Morana G, Piccardo A, Milanaccio C, et al. Value of 18F-3, 4-dihydroxyphenylalanine PET/MR image fusion in pediatric supratentorial infiltrative astrocytomas: a prospective pilot study. *J Nucl Med*. 2014;55(5):718–723.
11. Morana G, Piccardo A, Garrè ML, et al. Multimodal magnetic resonance imaging and 18F-L-dihydroxyphenylalanine positron emission tomography in early characterization of pseudoresponse and nonenhancing tumor progression in a pediatric patient with malignant transformation of ganglioglioma treated with bevacizumab. *J Clin Oncol*. 2013;31(1):e1–e5.
12. Alger JR, Frank JA, Bizzi A, et al. Metabolism of human gliomas: assessment with H-1 MR spectroscopy and F-18 fluorodeoxyglucose PET. *Radiology*. 1990;177(3):633–641.
13. Imani F, Boada FE, Lieberman FS, et al. Comparison of proton magnetic resonance spectroscopy with fluorine-18 2-fluoro-deoxyglucose positron emission tomography for assessment of brain tumor progression. *J Neuroimaging*. 2012; 22(2):184–190.
14. Hipp SJ, Steffen-Smith EA, Patronas N, et al. Molecular imaging of pediatric brain tumors: comparison of tumor metabolism using ^{18}F-FDG-PET and MRSI. *J Neurooncol*. 2012;109(3):521–527.
15. Floeth FW, Pauleit D, Wittsack HJ, et al. Multimodal metabolic imaging of cerebral gliomas: positron emission tomography with [18F]fluoroethyl-L-tyrosine and magnetic resonance spectroscopy. *J Neurosurg*. 2005;102(2):318–327.
16. Widhalm G, Krssak M, Minchev G, et al. Value of 1H-magnetic resonance spectroscopy chemical shift imaging for detection of anaplastic foci in diffusely infiltrating gliomas with non-significant contrast-enhancement. *J Neurol Neurosurg Psychiatry*. 2011;82(5): 512–520.
17. Stadlbauer A, Prante O, Nimsky C, et al. Metabolic imaging of cerebral gliomas: spatial correlation of changes in O-(2–18F-fluoroethyl)-L-tyrosine PET and proton magnetic resonance spectroscopic imaging. *J Nucl Med*. 2008;49(5):721–729.
18. Warren KE, Frank JA, Black JL, et al. Proton magnetic resonance spectroscopic imaging in children with recurrent primary brain tumors. *J Clin Oncol*. 2000;18(5):1020–1026.
19. Wen PY, Macdonald DR, Reardon DA, et al. Updated response assessment criteria for high-grade gliomas: response assessment in neuro-oncology working group. *J Clin Oncol*. 2010;28(11):1963–1972.
20. van den Bent MJ, Wefel JS, Schiff D, et al. Response assessment in neuro-oncology (a report of the RANO group): assessment of outcome in trials of diffuse low-grade gliomas. *Lancet Oncol*. 2011;12(6):583–593.
21. Sorensen AG, Patel S, Harmath C, et al. Comparison of diameter and perimeter methods for tumor volume calculation. *J Clin Oncol*. 2001;19(2):551–557.
22. Hourani R, Horská A, Albayram S, et al. Proton magnetic resonance spectroscopic imaging to differentiate between nonneoplastic lesions and brain tumors in children. *J Magn Reson Imaging*. 2006;23(2):99–107.
23. Marcus KJ, Astrakas LG, Zurakowski D, et al. Predicting survival of children with CNS tumors using proton magnetic resonance spectroscopic imaging biomarkers. *Int J Oncol*. 2007;30(3): 651–657.
24. Wilson M, Cummins CL, Macpherson L, et al. Magnetic resonance spectroscopy metabolite profiles predict survival in paediatric brain tumours. *Eur J Cancer*. 2013;49(2):457–464.
25. Girard N, Wang ZJ, Erbetta A, et al. Prognostic value of proton MR spectroscopy of cerebral hemisphere tumors in children. *Neuroradiology*. 1998;40(2):121–125.
26. García-Gómez JM, Luts J, Julià-Sapé M, et al. Multiproject-multicenter evaluation of automatic brain tumor classification by magnetic resonance spectroscopy. *MAGMA*. 2009;22(1):5–18.
27. Youland RS, Kitange GJ, Peterson TE, et al. The role of LAT1 in (18)F-DOPA uptake in malignant gliomas. *J Neurooncol*. 2013; 111(1):11–18.
28. Barker PB, Bizzi A, De Stefano N, et al. MR Spectroscopy in Brain Tumors. In: Barker PB, Bizzi A, De Stefano N, Guillapalli R, Lin DM eds. *Clinical MR Spectroscopy: Techniques and Applications*. New York: Cambridge University Press; 2010: 61–90.
29. Ledezma CJ, Chen W, Sai V, et al. 18F-FDOPA PET/MRI fusion in patients with primary/recurrent gliomas: initial experience. *Eur J Radiol*. 2009;71(2):242–248.

30. Tripathi M, Sharma R, D'Souza M, et al. Comparative evaluation of F-18 FDOPA, F-18 FDG, and F-18 FLT-PET/CT for metabolic imaging of low grade gliomas. *Clin Nucl Med*. 2009;34(12):878–883.
31. Kratochwil C, Combs SE, Leotta K, et al. Intra-individual comparison of ^{18}F-FET and ^{18}F-DOPA in PET imaging of recurrent brain tumors. *Neuro Oncol*. 2014;16(3):434–440.
32. Sala Q, Metellus P, Taieb D, et al. 18F-DOPA, a clinically available PET tracer to study brain inflammation? *Clin Nucl Med*. 2014; 39(4):e283–e285.
33. Herholz K, Hölzer T, Bauer B, et al. 11C-methionine PET for differential diagnosis of low-grade gliomas. *Neurology*. 1998; 50(5):1316–1322.
34. Tzika AA, Astrakas LG, Zarifi MK, et al. Spectroscopic and perfusion magnetic resonance imaging predictors of progression in pediatric brain tumors. *Cancer*. 2004;100(6):1246–1256.
35. Utriainen M, Metsähonkala L, Salmi TT, et al. Metabolic characterization of childhood brain tumors: comparison of 18F-fluorodeoxyglucose and 11C-methionine positron emission tomography. *Cancer*. 2002;95(6):1376–1386.
36. Mascelli S, Raso A, Biassoni R, et al. Analysis of NADP+-dependent isocitrate dehydrogenase-1/2 gene mutations in pediatric brain tumors: report of a secondary anaplastic astrocytoma carrying the IDH1 mutation. *J Neurooncol*. 2012; 109(3):477–484.